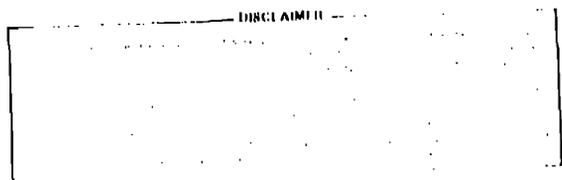**LA-UR** -82-2681

$Conf-8206118--6$

LA-UR--82-2681

DE83 000643

TITLE: A RESONANCE-FILTERED BEAM SPECTROMETER

MASTER

AUTHOR(S): R. M. Brugger, A. D. Taylor, C. E. Olsen, J. A. Gold
and A. K. Soper

—— DISCLAIMER ——

DISTRIBUTION OF THIS DOCUMENT IS UNLIMITED

Los Alamos

Los Alamos National Laboratory
Los Alamos, New Mexico 87545

ICANS-VI

INTERNATIONAL COLLABORATION ON ADVANCED NEUTRON SOURCES

June 27 - July 2, 1982

A RESONANCE-FILTERED BEAM SPECTROMETER

R.M. Brugger*, A.D. Taylor+, C.E. Olsen, J.A. Goldstone
and A.K. Soper

Physics Division
Los Alamos National Laboratory
Los Alamos, NM 87545

ABSTRACT

A new inelastic neutron scattering spectrometer which operates in the range 1 eV to 15 eV has been developed at the Los Alamos pulsed spallation source WNR. Based on a nuclear resonance filtering the beam, the concept has been tested in 'direct', 'inverted' and 'sample' geometries. A number of resonance filters have been tested to determine their effectiveness. The spectrometer is described and examples of data are presented.

*Permanent address: University of Missouri Research Reactor
                       University of Missouri
                       Columbia, MO

+Permanent address: Rutherford Appleton Laboratory
                       Chilton, Didcot
                       OXON OX11 OQX
                       United Kingdom

I. INTRODUCTION

The next generation of neutron sources, pulsed spallation sources, are now producing neutrons and scientific results[1]. These sources have a rich flux of epithermal neutrons which should open up unique research in the field of electron volt energy transfers. However, before this can be tested, spectrometers must be developed to explore this region. One such spectrometer, the resonance filtered beam spectrometer FBS is described in this paper[2,3].

II. PRINCIPLE OF OPERATION

The FBS uses a foil or filter with a strong nuclear resonance at E_R to define the energy of the incident (or scattered) neutrons. The scattered (or incident) energy is then found by time-of-flight TOF. The difference between TOF spectra taken without and with a filter in the beam gives the spectrum of scattered neutrons that would have had an incident (or final) energy corresponding to E_R. Thus the primary and secondary energies and momenta can be determined, and the conditions for performing an inelastic neutron scattering experiment are achieved. If the filter is in the incident beam, the geometry is called 'direct' while with the filter in the scattered beam, the geometry is called 'inverted.' A related arrangement, 'sample' geometry, where the system under investigation has a component with a nuclear scattering resonance has also beam tried, and is described.

III. RESOLUTION

The overall energy transfer resolution is a convolution of the contributions from the energy width of the resonance, incident and scattered flight path uncertainties and the moderated neutron pulse widths. These

contributions are, to a first approximation, for the direct geometry case, respectively

$$\Delta\epsilon^{(1)} = \left[1 + \frac{L_i}{L_f} \cdot \left(\frac{E_f}{E_i}\right)^{3/2}\right]\Delta E_R$$

$$\Delta\epsilon^{(2)} = 2 \cdot \frac{\Delta L_i}{L_f} \cdot \frac{E_f^{3/2}}{E_i^{1/2}}$$

$$\Delta\epsilon^{(3)} = 2 \cdot \frac{\Delta L_f}{L_f} \cdot E_f$$

$$\Delta\epsilon^{(4)} = 2 \cdot \frac{E_f^{3/2}}{2286\,L_f} \Delta t$$

The overall resolution is then

$$(\Delta\epsilon)^2 = \sum_i \left(\Delta\epsilon^{(i)}\right)^2 \quad .$$

In these equations, L_i and L_f are the incident and scattered flight paths and ΔL_i and ΔL_f their respective uncertainties. The energy width of the resonance filter's transmission is ΔE_R. The moderated neutron pulse width, Δt, is itself a convolution of contributions from neutron moderation Δt_m, and from the intrinsic width of the proton burst Δt_p where

$$\Delta t^2 = \Delta t_m^2 + \Delta t_p^2$$

or

$$\Delta t^2 \cong \frac{4000}{E} + \Delta t_p^2$$

Lengths are measured in meters, energies in meV and time in μs. For the inverted geometry case, these expressions become

$$\Delta\epsilon^{(1)} = \left[1 + \frac{L_f}{L_i} \cdot \left(\frac{E_i}{E_f}\right)^{3/2}\right]\Delta E_R$$

$$\Delta\epsilon^{(2)} = 2 \cdot \frac{\Delta L_i}{L_i} \cdot E_i$$

$$\Delta\epsilon^{(3)} = 2 \cdot \frac{\Delta L_f}{L_i} \frac{E_i^{3/2}}{E_f^{1/2}}$$

$$\Delta\epsilon^{(4)} = 2 \cdot \frac{\Delta L_f}{L_i} \frac{E_i^{3/2}}{2286 \, L_i} \Delta t$$

The above sets of equations indicate that the FBS in the direct geometry and inverted geometry are similar in resolution when flight paths can be optimized and energies are comparable. One practical consideration favoring the inverted geometry is that with the existing target shield it is quite difficult to make L_i short for the direct geometry while it is quite easy to make L_f short for the inverted geometry.

In addition to these explicit contributions to the energy transfer resolution, a defocusing effect is produced as the dispersion relationship for a given mass nucleus crossing the $Q-\epsilon$ locus for a resonance at a particular scattering angle. The effect may be seen in figure 1 (direct geometry) and figure 2 (inverted geometry). In these figures both the dispersion relation and the $Q-\epsilon$ loci which are illustrated as lines are, in reality, bands in $Q-\epsilon$ space.

IV. RESONANCE FILTERS

A search was made for nuclei with suitable resonances. Table I is a partial list of those which have been identified. It is important that the appropriate resonance is well separated from other resonances, that the resonant cross-section is high while the cross section beyond the resonance be relatively small. Also it is important that the resonance have a narrow natural width and a narrow Doppler width. Further criteria are that the material can be easily obtained elementally or isotopically and that it is easy to handle. The underlined cases in table I are those that have been, or are planned to be used at WNR. What is of importance in the measurement is not the cross-section but the transmission, so the resolution and intensity of a given resonance may be tuned by adjusting the filter thickness. As an example, ENDF/B-V cross-section data show the Doppler broadened widths of the 1.056 eV resonance of ^{240}Pu to be 58 meV at 300K and 43 meV at 77K. Such widths are only achievable in the limit of an infinitly thin absorber for which there would be no significant signal. Considerations of signal and resolution imply that at the resonance center an attenuation of about 0.75 is appropriate. Note that the optimum thickness for a given resonance is a function of the filter temperature. Figure 3 gives the variation of ΔE_R as a function of the filter thickness for ^{240}Pu. Data for Rh, Au and ^{238}U filters are given in figure 4. The solid points on the curves show the filter thicknesses at which the peak of the resonace gives 0.75 attentuation.

Table I shows that there are a number of available elements or isotopes that have narrow and isolated resonances. The limit to the resolution which can be achieved, set by the natural and Doppler widths of these resonances

is about 50 meV for 1 eV neutrons using a ^{240}Pu foil and 75 meV FWHM at 6.67 eV using a ^{238}U foil.

V. EXPERIMENTAL ARRANGEMENT

The three modes of this spectrometer have been developed and tested at WNR. Figure 5 shows the WNR target station and experimental area with the FBS set up in direct goemetry. On flight path 3 the incident flight path is about 5.5 m and the scattered neutrons are detected at about 5.5 m from the sample at an angle which may be varied between 0° and 120°. The unscattered beam is removed via the get lost pipe, thus reducing background.

Figure 6 shows the specta with the filter in and with the filter out when the sample was a thin slab of H_2O and a 0.002" thick sheet of Rh metal was the resonance filter. The scattering angle was 22°. At short times (less than 300μs) where the foil essentially attenuates no neutrons both spectra superimpose exactly. The dip in the foil in the spectrum at 700 μs corresponds to neutrons being absorbed from the primary beam at 1.257 eV by the Rh resonance. The difference between the two spectra, equivalent to scattering from an incident beam of 1.257 eV neutrons, is shown in figure 7.

The resolution function of this version of the spectrometer calculated for current WNR conditions using the equations of section III is given in figure 8 for a variety of resonance filters. It should be noted that the WNR proton pulse of about 4 μs (contribution $\Delta\epsilon^{(4)}$) dominates the ^{238}U resolution, is an equal contribution to the resolution when Au is the filter, but does not effect the resolution functions when either Rh or ^{240}Pu are the filters.

Figure 9 shows the FBS set up in its inverted geometry mode on flight path 11. In this configuration the incident flight path of about 30 m

provides excellent TOF resolution. The filter is placed in the scattered beam, thus defining the final energy. A short secondary flight path further improves the resolution. Detectors are time analyzed independently to improve Q resolution by limiting the angular resolution. The form of the resolution function for this spectrometer is given in figure 10.

An earlier trial version of the inverted geometry mode on flight path 3 used a 5.5 m incident flight path and a 1.4 m secondary flight path. The energy resolution of this configuration is given in figure 11. The large solid angle accepted by the ganged detectors in this case degraded the Q resolution. Figure 12 shows spectra obtained in this inverted geometry when the sample was 1mm of ZrH_2 and the filter was 0.002" of Rh. The top spectrum is for no filter in the final beam and the middle spectrum is the response with Au in the final beam. The bottom spectrum is the difference. One sees "elastic" scattering from the Zr at channel 1100 while the inelastic scattering from the H is near channel 800. Each spectrum was run for 20 μA-hr.

Figure 13 shows the FBS set up in the sample geometry. In this arrangement, the energy defining resonance is part of the sample and no additional filter is used. Figure 14 shows the scattering spectrum from a 0.001" thick sample of UO_2. Peaks from the 6.674 eV, 20.90 eV, 36.80 eV, 102.47 eV and 208.46 eV scattering resonances are observed on top of a background from the fast neutron burst. The resonances define an interaction energy while the energy after scattering is measured by TOF over the secondary flight path of 5.5 m. Thus information about the recoil energy and broadening of the resonance caused by binding effects can be determined.

The spectra presented in the proceeding paragraphs show the versatility of FBS and that it can operate in all three geometries.

VI. SCATTERING EXPERIMENTS

The goals of developing eV spectrometers are to study high energy excitations, excitations that show the ground state momentum distribution of particles, transitions between magnetic states of crystals, and transitions between electronic states of materials. Many of these experiments are difficult and beyond the initial capabilities of FBS or any other eV spectrometer. More accessable experiments were tried first to show the capability of an FBS.

An easy class of experiment is found by scattering from atoms of mass 1 amu, where the widths of the inelastic scattering are correspondingly greater. Scattering at high Q gives a direct observation of the ground state momentum distribution of the H atom and hence leads to the shape of the potential the proton experiences. Such measurements are clearly of importance in understanding, for example, hydrogen bonded systems.

As a preliminary experiment, the ground state momentum distribution of ZrH_2 was investigated where the potential is well described by a simple harmonic oscillator of frequency 140 meV. Figure 15 shows data for scattering from ZrH_2 at 90° using a 0.002" Rh foil. The sharp peak at channel 45 corresponds to recoil scattering from Zr atoms and the broad feature centered at channel 66 is due to scattering from H. The width of the Zr peak corresponds to the calculated resolution function. The dashed line corresponds to scattering from a simple harmonic oscillator of frequency 150 meV. evaluated along a constant scattering angle of 90°. The resolution

function for the Rh foil has been folded in. The actual position of the maximum in scattering from H is an artifact of the cut taken thru Q-ε space and the shape of S(Q,ε). This position is very sensitive to the width of the scattering function. Figure 16 shows an inverted geometry measurement made on the same system with a 0.002" Rh filter and the detectors at 60°, (using the short FP 3 configuration). These data have been transformed to an energy transfe scale. Again the sharp peak at ε = 0 eV is Zr scattering and its width is in excellent agreement with the calculation shown in figure 11. The broad H mode centered at ε = 1.5 eV is again consistent with a simple harmonic oscillator of frequency 150 meV. This time the peak does reflect a maximum in S(Q,ε). Detailed analysis of these data was not carried out due to the large (± 6°) acceptance of the detector bank in the trial geometry.

Scattering at large Q requires large scattering angles, thus removing detector from regions of high background. The physics processes in the system of interest tend to broaden with Q and so energy and resolution requirements become less severe. Figure 17 shows the high Q scattering from a series of different mass nuclei. The FBS ...as in direct geometry with the scattering angle 117.5° and the foil was 0.003" of ^{238}U. In these data,

shifts in peak position due to recoil, $\epsilon_R = \dfrac{\hbar^2 Q^2}{2M}$ are evident. The effect being greatest for the mass 4 amu case. Although for these particular run conditions the width of each peak was dominated by instrumental resolution, the effect of resolution is again least for He. By fitting the He data, a ground state momentum distribution of the struck particles (normal He) was obtained. The He peak has a width corresponding to an effective temperature of 13K, in agreement with previous measurements. The resolution, figure 8, of this geometry was, however, too poor to attempt to separate the condensate and noncondensate fractions for He below the lambda point.

Two approaches are possible to improve the charactistics of the He experiment. By using the inverted geometry, with a long primary flight path and by using short proton burst (0.5 μs) all contributions to the resolution can be made small relative to the intrinsic energy width of the resonance. For a 30 m primary path and a 1 m secondary path, some 100 meV resolution may be achieved at a final energy of 6.67 eV corresponding to the ^{238}U resonance. The second device which may be employed to improve the experiment is, that by going to the inverted technique ($E_i > E_f = E_R$), Q can be increased since E_f is larger. This expands the characteristic widths of both distributions, which are proportional to Q, relative to the intrinsic resolution, which has a much weaker dependence on Q. Figure 18a, illustrates the cut taken thru Q-ϵ space and Figure 18b shows simulated data including a statistical variance appropriate to the subtraction technique for a 10% condensate fraction. A fit to these simulated data (solid and dashed lines) allows the two components of this lineshape to be extracted, recovering, within resonable errors, the simulated condensate fraction and the condensate and noncondensate widths.

Figure 19 gives an example of a sample geometry experiment. The two peaks correspond to scattering from the 6.674 eV resonance in U when the U atoms are bound in UO_2 and UF_4. Within the present resolution, the same recoil energy and widths are measured for both materials.

The above examples of data show that a certain class of experiments using eV neutrons on FBS are now possible. The results also provide encouragement to attempt the more difficult experiments such as observing magnetic

transitions for which Q must be $< 4 \text{ Å}^{-1}$ while ϵ will be greater than 100 meV. Similar measurements to observe electronic excitations in molecules will require $Q < 4 \text{ Å}^{-1}$.

VII. CONCLUSIONS

The results presented in the preceeding sections show that FBS works as an inelastic neutron spectrometer with eV neutrons. Its major disadvantages are: 1) that the statistical accuracy of each point is limited because FBS employs a difference to define an event and 2) the resolution is limited by the energy width of the nuclear resonance used as a filter.

The general advantages of FBS are: 1) it is relatively easy to assemble and use, 2) it can be used in all three geometries, 3) counting rates can be large which helps to overcome the difference disadvantage, 4) the subtraction technique removes fast neutron background, 5) a large number of resonances are available, 6) the foils are relatively easy to handle and cool, and 7) since only neutrons are detected, filters that are radioactive can be used.

Both the direct and inverted geometry configurations have their merits. In the direct geometry, the necessity of having a long secondary flight path may be capitalized on for low Q scattering where a reasonable radial separation between beam and detector may be achieved at small angle. A further advantage of the filter being in the primary beam is that only a small filter area is required and so smaller (and hence more esoteric) filters may be used. Cooling the filters to suppress Doppler broadening is also facilitated. The inverted geometry has the advantage that the long initial flight path fits well with the biological shielding requirement. In many cases, the direct and indirect geometries complement each other.

References

1. C. G. Windsor, <u>Pulsed Neutron Scatttering</u>, Taylor and Francis Ltd, London (1981).

2. R. M. Brugger, A. D. Taylor, C. E. Olsen and J. A. Goldstone, Bulletin of the APS, <u>27</u>, #1, pp 13 (Jan 1982).

3. A. D. Taylor and R. M. Brugger, Bulletin of the APS, <u>27</u>, #1, pp 14 (Jan 1982).

Acknowledgements

FIGURE CAPTIONS

Figure 1.   For direct geometry, the cut in Q-ϵ space of inelastic scattering for particular incident energies (Rh, Au, U) at particular angles (22°, 60°, 90°, 117°) by particular mass particles (1, 4, 9, 27 amu).

Figure 2.   For indirect geometry, similar cuts in Q-ϵ space to Figure 1.

Figure 3.   For ^{240}Pu, the variation of the observed resonance width ΔE_R as a function of filter thickness. The solid points represent thicknesses that give 0.75 attenuation at the center of the resonance.

Figure 4.   For Rh, Au and U, the variation of the observed resonance width ΔE_R as a function of filter thickness. The solid points represent thicknesses that give 0.75 attenuation at the center of the resonance.

Figure 5.   The WNR target station and experimental area with the FBS in direct geometry at flight path 3.

Figure 6.   For direct geometry, the spectra with filter out and filter in when neutrons are scattered at 22° from a thin H_2O sample and the filter is 0.002" Rh.

Figure 7.   The difference of the two spectra of Figure 6.

Figure 8.   Calculated resolution of the FBS for direct geometry as structured in Figure 5.

Figure 9.   The WNR target station and experimental area with the FBS in inverted geometry at flight path 11.

Figure 10. Calculated resolution of FBS in inverted geometry as structured in Figure 9.

Figure 11. Calculated resolution FBS in inverted geometry at flight path 3.

Figure 12. For inverted geometry, the spectra taken at flight path 3 for a 1 mm thick sample of ZrH_2 and with a filter of 0.002" Rh. The detectors observed scattering at 60°.

Figure 13. The WNR target station and experimental area with the FBS in sample geometry at flight path 3.

Figure 14. For sample geometry, the spectrum observed for scattering at 117° from a sample of UO_2 which is 0.001" thick.

Figure 15. Scattering data for a 1 mm thick sample of ZrH_2. The scattering was at 90° and the filter was 0.002" Rh in direct geometry.

Figure 16. Scattering data from the 1 mm thick sample of ZrH_2. The scattering was at 60° and the filter was 0.002" Rh in inverted geometry at flight path 3.

Figure 17. Scattering data from samples of Pb, Al, liquid N_2 and liquid He. The scattering was at 117.5° and the filter was 0.003" ^{258}U in direct geometry.

Figure 18. a) The cut in Q-ε space for scattering from He. The filter is ^{238}U in inverted geometry.

b) A simulated curve for scattering from He (90% normal and 10% condensed phase).

Figure 19 Example of data for sample geometry. The samples were $^{238}UO_2$ and $^{238}UF_4$ about 0.001" thick. The scattering was at 117.5°. The squares are UO_2 and the circles are UF_4.

TABLE I

Some Possible Resonances for FBS

Isotope	Natural Abundance (%)	E_R (eV)	Nuclear Width (meV)	Doppler-Broadened Width (meV)	Peak Cross Section (Temperature) (barns (K))
^{149}Sm	13.9	0.872	61		2790(300)
^{240}Pu	-	1.056	33.3	58	112000(300)
^{240}Pu	-	-	-	43	139000 (77)
^{103}Rh	100	1.257	156	178	4081(300)
^{193}Ir	62.7	1.303	87.3		5830(300)
^{115}In	95.7	1.457	75		29900(300)
^{185}Re	37.4	2.156	57.7		9300(300)
^{242}Pu	-	2.67	27		35200(300)
^{238}Pu	-	2.90	38		1020(300)
^{169}Tm	100	3.90	108		30100(300)
^{181}Ta	100	4.28	57		14100(300)
^{197}Au	100	4.906	139	180	30800(300)
^{234}U	-	5.19	29		27500(300)
^{236}U	-	5.45	27		15700(300)
^{238}U	99.3	6.674	27.5	104	7712(300)
^{238}U	-	-	-	54	12475 (77)
^{238}Pu	-	9.98	42		4200(300)
^{159}Tb	100	11.14	95		7140(300)
^{195}Pt	33.8	11.9	127		3120(300)
^{163}Dy	24.9	16.23	124		2070(300)
^{186}W	28.6	18.84	337		29800(300)
^{238}U	99.3	20.90	34	-	8510(300)

NEUTRON
SOURCE

FILTER

SAMPLE

FP 5

FP 4

FP 3

DETECTORS 117.4°

NP

FP 12

FP 1

DETECTORS 21.8°

GET LOST PIPE

FP 2

5 METERS

FP8
FP7
FDS
FP6
FP5
FP 4
FP 3

FP 9
FP10
FP 11
NEUTRON SOURCE

NP
NP
NP
FP12
FP 1
FP 2

DETECTORS
FILTER
SAMPLE

5 METERS

Au (0.001 in.)

Rh (0.002 in.)

^{238}U (0.003 in.)

^{240}Pu (4mg cm^{-2})

$\Delta \epsilon$ (meV)

ENERGY TRANSFER, ϵ (meV)

NEUTRON
SOURCE

SAMPLE

FP 5

FP 12

DETECTORS 117.4°

NP

FP 4

FP 1

DETECTORS 21.8°

FP 3

GET LOST PIPE

FP 2

5 METERS

ZrH$_2$ 5mil Rh   Filter

- - - - SHO   M = 1

$\omega_0 = 150$ meV

INTENSITY

CHANNEL (16us)

ZrH₂   2 mil   Rh   Inverted   Geometry